J A C S
JOURNAL OF THE AMERICAN CHEMICAL SOCIETY

NOTTINGHAM
TRENT UNIVERSITY

Subscriber access provided by Nottingham Trent University

Article

Thermodynamic Analysis of Metal-Ligand Cooperativity of PNP Ru Complexes: Implications for CO Hydrogenation to Methanol and Catalyst Inhibition

Cheryl L. Mathis, Jackson Geary, Yotam Ardon, Maxwell S. Reese,
Mallory A. Philliber, Ryan T VanderLinden, and Caroline T. Saouma

J. Am. Chem. Soc., **Just Accepted Manuscript** • DOI: 10.1021/jacs.9b06760 • Publication Date (Web): 07 Aug 2019

Downloaded from pubs.acs.org on August 8, 2019

Just Accepted

“Just Accepted” manuscripts have been peer-reviewed and accepted for publication. They are posted online prior to technical editing, formatting for publication and author proofing. The American Chemical Society provides “Just Accepted” as a service to the research community to expedite the dissemination of scientific material as soon as possible after acceptance. “Just Accepted” manuscripts appear in full in PDF format accompanied by an HTML abstract. “Just Accepted” manuscripts have been fully peer reviewed, but should not be considered the official version of record. They are citable by the Digital Object Identifier (DOI®). “Just Accepted” is an optional service offered to authors. Therefore, the “Just Accepted” Web site may not include all articles that will be published in the journal. After a manuscript is technically edited and formatted, it will be removed from the “Just Accepted” Web site and published as an ASAP article. Note that technical editing may introduce minor changes to the manuscript text and/or graphics which could affect content, and all legal disclaimers and ethical guidelines that apply to the journal pertain. ACS cannot be held responsible for errors or consequences arising from the use of information contained in these “Just Accepted” manuscripts.

is published by the American Chemical Society. 1155 Sixteenth Street N.W.,
Washington, DC 20036

Published by American Chemical Society. Copyright © American Chemical Society.
However, no copyright claim is made to original U.S. Government works, or works
produced by employees of any Commonwealth realm Crown government in the course
of their duties.

Thermodynamic Analysis of Metal-Ligand Cooperativity of PNP Ru Complexes: Implications for CO_2 Hydrogenation to Methanol and Catalyst Inhibition

Cheryl L. Mathis, Jackson Geary, Yotam Ardon, Maxwell S. Reese , Mallory A. Philliber, Ryan T. VanderLinden and Caroline T. Saouma*

Department of Chemistry, University of Utah, 315 S. 1400 E., Salt Lake City, Utah 84112, U.S.A.

Supporting Information Placeholder

ABSTRACT: Hydrogenation of CO_2 in the presence of amines to formate, formamides, and methanol (MeOH) is a promising approach to streamline carbon capture and recycling. To achieve this, understanding how catalyst design impacts selectivity and performance is critical. Herein we describe a thorough thermochemical analysis of the (de)hydrogenation catalyst, **(PNP)Ru-Cl** (PNP = 2,6-bis-(di-*tert*-butylphosphinomethyl)pyridine; Ru = Ru(CO)(H)), and correlate our findings to catalyst performance. While this catalyst is known to hydrogenate CO_2 to formate with a mild base, we show that MeOH is produced when using a strong base. Consistent with pK_a measurements, the requirement for a strong base suggests that deprotonation of a 6-coordinate Ru species is integral to the catalytic cycle that produces MeOH. Our studies also indicate that the concentration of MeOH produced is independent of catalyst concentration, consistent with a deactivation pathway that is dependent on methanol concentration, not equivalency. Our temperature-dependent equilibrium studies of the dearomatized congener, **(*PNP)Ru**, with various H-X species (to give **(PNP)Ru-X**; X = H, OH, OMe, OCHO, OC(O)NMe$_2$) reveal that formic acid equilibrium is ~ temperature independent; relative to H_2, it is more favored at elevated temperatures. We also measure the hydricity of **(PNP)Ru-H** in THF and show how subsequent coordination of the substrate can impact the apparent hydricity. The implications of this work are broadly applicable to hydrogenation and dehydrogenation catalysis and in particular, those that can undergo metal-ligand cooperativity (MLC) at the catalyst. These results serve to benchmark future studies by allowing comparisons to be made amongst catalysts and will positively impact rational catalyst design.

INTRODUCTION

Rising atmospheric carbon dioxide levels present a significant incentive to develop new catalysts that are active for the transformation of CO_2 into renewable fuels. Catalysts that engage in metal-ligand cooperativity (MLC)[1] are particularly attractive due to their proven ability to hydrogenate CO_2 to formate;[2,3,4] in the presence of amines, formamides[5,6] and MeOH are also produced.[7,8] Formic acid and MeOH are both attractive to probe as hydrogen storage mediums.[9] However, existing studies often employ high pressures/temperatures, strong bases, and precious metals to promote reactivity. A thermochemical understanding of existing systems will help guide the rational design of next generation catalysts; factors such as *pK$_a$* of the ligand, K_{eq} with substrates, and ΔG_{H^-} can all modulate catalyst performance.

The strategy of MLC is illustrated in Figure 1, which considers the hydrogenation of CO_2 to formate with Milstein's PNN-ligated Ru catalyst.[2a] In this mechanism, H_2 is heterolytically cleaved with ligand protonation concomitant to hydride installation on Ru. While this mechanism has been proposed by Sanford,[2a] the direct pathway is suggested by Pidko in the analogous PNP-ligated Ru system (Figure 1, right pathway).[2c] Their calculations suggest that deprotonation of the bound H_2 in a cationic Ru-H_2 species occurs with the added base and an outer-sphere formate. Their analysis moreover suggests that the species with formate bound to the Ru is an off-cycle species, contrary to the MLC pathway. These cycles illustrate how hydricity, pK_a, and propensity to react with H_2 over other H-X species must be balanced. Related computational studies suggest that the direct pathway may be more favorable than those that undergo MLC with both Ru and Ir catalysts,[2c,10] but the calculations do no always take into account the reaction conditions. These discrepancies reinforce the need to experimentally establish the thermodynamic parameters of such systems to determine their impact on catalysis.

For the successful hydrogenation of CO_2 to MeOH,[11] only catalysts that can or are speculated to undergo MLC

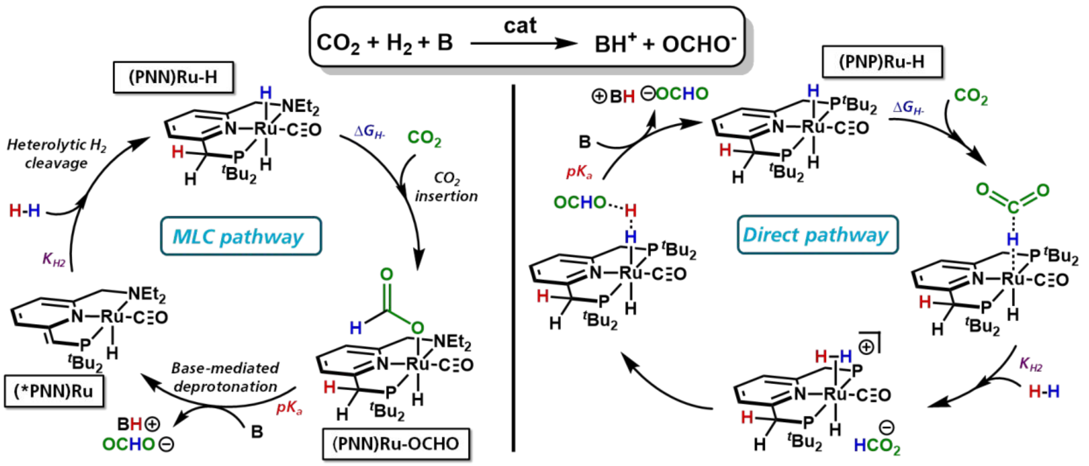

Figure 1. Mechanistic proposals for the hydrogenation of CO_2 to formate. All Ru species are L_4X_2 and 18 e^-. Pertinent thermochemical parameters are given outside the reaction arrows. **(left):** MLC mechanism, whereby H_2 addition occurs to the dearomatized **(*PNN)Ru**. **(right):** The direct pathway does not undergo ligand deprotonation.

facilitate this transformation in the presence of amines.[7-8] This is pertinent to carbon capture and recycling schemes, as current technologies rely on amines to capture CO_2, giving carbamates and carbonates.[12] However, these systems are limited by the energetic demands required for CO_2 release.[13] Thus, hydrogenation of CO_2 in the presence of amines would streamline carbon-capture and recycling.

Hydrogenation of carbamates ("captured CO_2") is thought to occur via thermal release of CO_2, which is first hydrogenated to formate (Scheme 1, (i)).[7b,14] Condensation with an amine then provides formamide, which is further hydrogenated to MeOH (Scheme 1, (ii)). Not all catalysts that hydrogenate CO_2 to formate can hydrogenate formic acid to MeOH (in the presence of amines),[7d] and generally harsher conditions are required for the latter.[5,8b] Sometimes, the CO_2 must first be removed and hence the overall transformation is necessarily sequential.[8b] For Ru, it is speculated that only hydrogenation of formamide to MeOH occurs via MLC (Scheme 1, step (ii)),[14] whilst with Mn both steps are thought to proceed via MLC.[8b] Establishing the mechanism for both hydrogenations as well as the thermodynamic parameters of catalysts that can and cannot do this transformation are warranted to advance catalyst development.

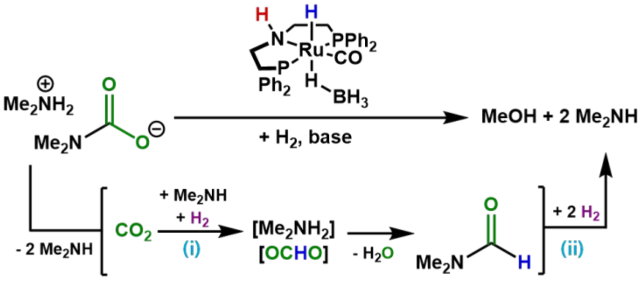

Scheme 1. Hydrogenation of (DMA-H)(DMC) to MeOH is mediated by aliphatic **$(^{Ph}P^{H}NP)$Ru-(HBH_3)** that can undergo MLC. The hydrogenation is thought to proceed via the species shown, with the hydrogenation steps labelled (i) and (ii).

Towards advancing catalysts that transfer net H_2, several systems that undergo MLC have been developed.[1c] Comparisons of catalyst performance often are based on turnover numbers (TON), turnover frequencies (TOF), and/or reaction times.[1c] With no further mechanistic studies, these parameters do not reveal the underlying reason(s) as to why the catalysts perform differently, nor do they correlate these effects with thermochemical parameters, limiting rational catalyst design.

Recently, Prakash and co-workers investigated the role of the ligand and amine additive for hydrogenation of CO_2 to MeOH.[14] They found a correlation between how electron-donating the pincer ligand is to the catalyst performance, and through elegant mechanistic studies, established that this is due to the relative stability of an off-cycle species.

As the catalyst is implicated in each step of the mechanism, it is important to know the thermodynamic parameters associated with the catalyst. Hydricity, basicity, and ease of cleaving an H-X bond (Figure 1) are likely sensitive to modification of the catalyst. This approach has been applied to electrocatalytic H_2 evolution[15] and CO_2 reduction.[16] Expanding this knowledge to hydrogenations,[17] particularly those that undergo MLC, will help develop catalysts whereby each step is energetically ~ thermoneutral, avoiding highly exothermic and subsequent endothermic steps. It will also shed light on potential inhibition pathways, which may clarify the correlation of catalyst loading and TON. The results will be broadly applicable to systems that transfer H_2.

Herein we provide a thorough thermochemical analysis of the Ru PNP system. This catalyst is chosen for these studies as it can perform several dehydrogenations[18] and hydrogenations[19] including that of CO_2 to formate,[2c,2d,20] and in the presence of amines, MeOH (*vide infra*). The analysis presented provides the first hydricity measurements in THF and the first hydricity measurements for complexes that react via MLC.[21] This work also considers how coordination of a 6th ligand impacts the apparent hydricity and pK_a of the catalyst, and participation in likely thermodynamic bottlenecks during catalysis. Finally, the thermodynamic values are correlated to catalytic results. Overall, this study benchmarks the thermodynamic parameters for (de)hydrogenation catalysts that operate via MLC. This allows for future comparisons to be made and understanding of catalyst limitations.

RESULTS

Overview of system considered. The (PNP)Ru species pertinent to this study are shown in Figure 2 (PNP = 2,6-bis-(di-*tert*-butylphosphinomethyl)pyridine). Central to all the equilibria is the 5-coordinate dearomatized species, **(*PNP)Ru** (Figure 2, middle top).[18a] This species reacts with Brønsted acidic H-X species to give **(PNP)Ru-X** ($K_{1,X}$); in this reaction proton transfer to the ligand is coupled to nucleophilic attack of X^- to Ru (Figure 2, bottom left).[1c] These equilibria are pertinent as they are competitive with addition of H_2 or other species to **(*PNP)Ru** in the catalytic cycle (Figure 1).

The cationic L_3X_2 16-electron species, **[(PNP)Ru]$^+$**,[22] is the protonated congener of **(*PNP)Ru** and is related to **(PNP)Ru-X** by loss of the anionic X-type ligand (Figure 2, bottom). Thus, it is the product of hydride transfer to a substrate. These three congeners are readily accessible synthetically, and when X = H, together they are used to establish the hydricity of **(PNP)Ru-H** (Figure 2, bottom left).

Deprotonation of **(PNP)Ru-X** gives [(***PNP)Ru-X]$^-$**, a formally L_5X_2 20-electron species. With few exceptions,[2a,22-23] species of the type [**(*PNP)Ru-X]$^-$** are not stable and lose X^-,[1c] yielding **(*PNP)Ru**. For example, treatment of **(PNP)Ru-Cl** with 1 equiv of KO^{t}Bu gives dearomatized **(*PNP)Ru**.

Dearomatized **(*PNP)Ru** also reacts with Lewis acids[23] such as CO_2 to give **(PNP)Ru-CO$_2$**,[24] whereby the basic site on the ligand attacks the Lewis-acidic carbon of CO_2 (Figure 2, bottom right). This species is speculated to be detrimental to hydrogenation of CO_2.[2a,2d] The adduct can also be deprotonated to give **[K][(*PNP)Ru-CO$_2$]** (*vide infra*).

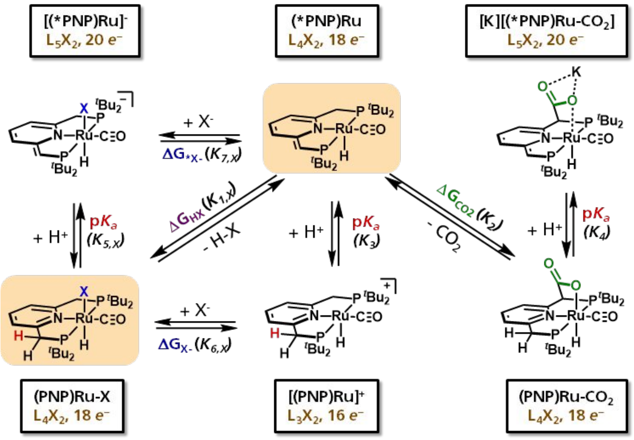

Figure 2. Thermodynamic parameters considered in this study. Species in gold boxes are proposed to be pertinent to catalysis via MLC (Figure 1). Equilibrium constants are shown above the arrow that corresponds to the direction of *K*. For clarity, only balanced equations are shown for the reverse equilibria. As all the congeners feature a hydride and a CO ligand that remain unchanged, we do not include these ligands in the shorthand nomenclature (boxed), and simply give the identity of the X-type ligand that occupies the 6th coordination-site. Deprotonation of the PNP ligand at one of the methylene positions gives the dearomatized species (indicated by *), whereby the pyridine L-type donor becomes an anionic LX-type donor. Formal ligand type and electron count are provided in the boxes for clarity.

Synthesis and characterization of complexes. Towards measuring the equilibria shown in Figure 2, several pertinent congeners needed to be prepared. Addition of H_2, Brønsted acidic H-X or Lewis acidic CO_2 to **(*PNP)Ru** readily gives **(PNP)Ru-X** (Figure 2), as described in the literature (X = H, OMe, OCHO, OH).[2d,5,24] It should be noted that in the presence of Lewis or Brønsted acids, **(*PNP)Ru** is in equilibrium with **(PNP)Ru-X**, where the equilibrium constant depends on the identity of H-X and in some instances, the concentration (*vide infra*). Thus, the various proton sources that may be produced during catalysis are in competition with H_2 to coordinate the metal (i.e., competing $K_{1,X}$) during catalysis.

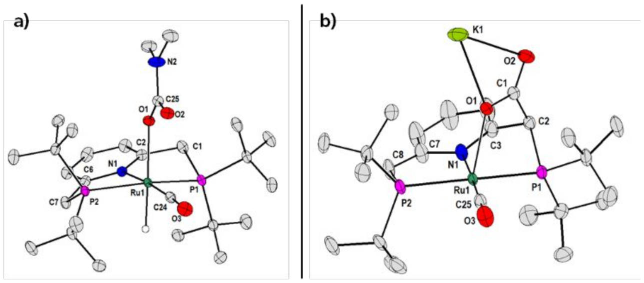

Figure 3. Solid-state structures (50% displacement ellipsoids) of **a) (PNP)Ru-DMC** and **b) [K][(*PNP)Ru-CO$_2$].** All calculated hydrogen atoms and minor components of disorder are omitted for clarity. Only one half of the dimeric unit of **[K][(*PNP)Ru-CO$_2$]** is shown. Select bond distances (Å) for **(PNP)Ru-DMC**: Ru1-N1 2.145(1), Ru1-O1 2.205(1), C1-C2 1.503(2), C6-C7 1.495(2). Select bond distances (Å) for **[K][(*PNP)Ru-CO$_2$]**: Ru1-N1 2.119(3), Ru1-O1 2.331(3), C1-O1 1.269(5), C1-O2 1.244(5), C1-C2 1.552(6), C2-C3 1.510(6), C7-C8 1.374(6). Analogous bonds in the other half of the dimer have similar bond distances.

To probe the initial Ru species formed in catalytic hydrogenation of amine "captured" CO_2,[5,7,14,25] we sought to prepare a carbamate species. Addition of excess of dimethylammonium dimethylcarbamate, (DMA-H)(DMC), to dearomatized **(*PNP)Ru** cleanly generates **(PNP)Ru-DMC**. This carbamate was chosen because (DMA-H)(DMC) has been shown to be hydrogenated to MeOH using **(^{Ph}P^{H}NP)Ru-(HBH$_3$)** as a catalyst (Scheme 1).[7b] The identity of **(PNP)Ru-DMC** as a 6-coordinate aromatized species was confirmed by NMR spectroscopy and XRD (Figure 3). Similar to other carboxylate bound species such as **(PNP)Ru-OCHO**[2d] and **(PNP)Ru-CO$_2$**,[24] the hydride resonance appears as a triplet centered at δ = -16.74 ppm (J_{PH} = 19 Hz) in the ^{1}H NMR spectrum (d_8-THF). Though the carbamate species **(PNP)Ru-DMC** is in equilibrium with **(*PNP)Ru** (*vide infra*), it is stable to vacuum. This is also true for the other carboxylate species, **(PNP)Ru-OCHO** and **(PNP)Ru-CO_2**, but contrasts the instability of **(PNP)Ru-H**, **(PNP)Ru-OH,** and **(PNP)Ru-OMe**, all of which revert to dearomatized **(*PNP)Ru** upon concentration *in vacuo* at ambient temperature;[26] this instability limits our ability to readily isolate these species in the absence of H-X in solution.

To gain insight into the true pK_a of 6-coordinate **(PNP)Ru-X**, we sought to deprotonate **(PNP)Ru-CO_2**. The rationale being that the Ru-O bond will be weakened or if cleaved, will remain formally associated with the Ru (Figure 2).[2a] This is in contrast to the other **(PNP)Ru-X** species which lose X^- and therefore have a ΔG_{*X-} contribution (Figure 2, top left to top middle). Indeed, reaction of a d_8-THF solution of **(PNP)Ru-CO_2** with 1 equiv of KHMDS (KHMDS = potassium hexamethyldisilazide) cleanly gives **[K][(*PNP)Ru-CO_2]**. The NMR spectral parameters for this species are similar to that of **[(*PNN)Ru-CO_2]$^-$** which was characterized by Sanford and coworkers[2a] (see Figure 1 for PNN structure and SI for NMR characterization).

To determine if the CO_2 oxygen remained bound to the Ru or not, crystals of **[K][(*PNP)Ru-CO_2]** were grown by vapor diffusion of diethyl ether into THF, and the solid-state structure is shown in Figure 3. In the solid-state, **[K][(*PNP)Ru-CO_2]** is a dimeric species bridged by a K_2O_2 diamond core (see SI). The loss of aromaticity is evident from the C7-C8 bond distance of 1.374(6) Å. By contrast, C2-C3 is 1.510(6) Å, which is similar to that found in the neutral analogue (1.507(2) Å).[24] Upon deprotonation, the N1-Ru1 bond distance remains unchanged (Figure 3 caption). This contrasts with deprotonation of the related aliphatic PNP ligands (Scheme 1), whereby the amide-Ru bond distance is noticeably shorter (~0.18 Å) than the amine-Ru bond distance.[27] Notably, CO_2 still coordinates to Ru with a Ru1-O1 bond distance of 2.331(3) Å. This represents a ~ 0.05 Å elongation from neutral **(PNP)Ru-CO_2**[24] and a ~ 0.07 – 0.1 Å elongation from other structurally characterized carboxylate and carbonate derivatives.[2d] The observed elongation is consistent with the Ru center now being formally 20-electron.

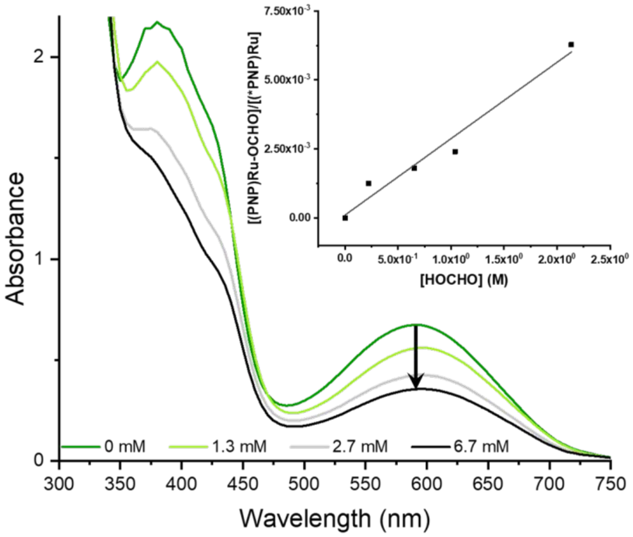

Figure 4. Stacked UV-vis spectra for the equilibria of **(*PNP)Ru** (0.60 mM) and formic acid in THF. Concentrations of formic acid given in the legend are those at equilibrium. **(inset):** Plot of $\frac{[(\mathbf{PNP})\mathbf{Ru}-\mathbf{OCHO}]}{[(^*\mathbf{PNP})\mathbf{Ru}]}$ vs. [H-OCHO]. The slope gives $K_{1,OCHO}$ (eq 1).

Equilibria with H-X species. Dearomatized **(*PNP)Ru** readily reacts with Brønsted and Lewis acids to give **(PNP)Ru-X** (Figure 2, $K_{1,X}$ and K_2, respectively). However, given the importance of its reaction with H_2 for hydrogenation reactions, and the potential inhibitory effect of this reaction with other species that may be present during catalysis, we sought to establish the equilibrium constants with H_2, H-X ($K_{1,X}$), and CO_2 (K_2). Our interest in hydrogenation of CO_2 prompted analysis of the following H-X species that may be present during catalysis: MeOH, H_2O, HC(O)OH, DMF, diethylamine, and [DMA-H][DMC]. Neither DMF nor diethylamine reacts with **(*PNP)Ru** to an observable extent (see Figures S39, S35, respectively); all other species react with **(*PNP)Ru** to give **(PNP)Ru-X**. The equilibrium is readily monitored by UV-vis spectroscopy by observing the absorbance at 595 nm, which corresponds to dearomatized **(*PNP)Ru** (Figure 4). Briefly, addition of various concentrations of H-X to a THF solution of **(*PNP)Ru** allows for the equilibrium constant (eq 1) to be established.

$$(1)\quad (K_{1,X}) = \frac{[(\mathbf{PNP})\mathbf{Ru}\text{–}\mathbf{X}]}{[(^*\mathbf{PNP})\mathbf{Ru}]\cdot[\text{H–X}]}$$

Equation 1 represents the binding of H-X to the Ru and the stoichiometry suggests that there should be a concentration-dependence to the equilibrium constant. This is confirmed by diluting equilibrium samples and noting the shift in the ratio of the two Ru species (see SI). Apart from (DMA-H)(DMC) (eq 2-3), this concentration-dependence was observed for all H-X species.

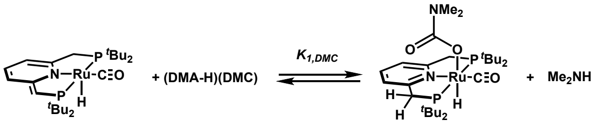

(2)

$$(3)\quad K_{1,DMC} = \frac{[(\mathbf{PNP})\mathbf{Ru}\text{–}\mathbf{DMC}]\cdot[\text{DMA}]}{[(^*\mathbf{PNP})\mathbf{Ru}]\cdot[(\text{DMA–H})(\text{DMC})]}$$

The lack of concentration-dependence for the equilibrium with (DMA-H)(DMC) is rationalized on the basis that one equivalent of DMA is formed and the (DMA-H)(DMC) substrate is strongly ion-paired in solution.

Similarly, the equilibrium constant for the binding of H_2 and CO_2 is measured analogously (eqs 4 and 5, respectively), with the gas pressures given in atm. These measurements necessitate knowledge of the equilibrium partial pressure due to the gas, and hence require a large head-space such that minimal changes occur during equilibration (see SI for details). At pressures that we can accurately measure, no **(*PNP)Ru** is observed at room temperature for the equilibria with H_2 or CO_2; the equilibrium constants are therefore extrapolated from higher temperature data (*vide infra*).

$$(4)\quad (K_{1,H}) = \frac{[(\mathbf{PNP})\mathbf{Ru{-}H}]}{[(^*\mathrm{PNP})\mathbf{Ru}]\cdot \mathrm{pH_2}}$$

$$(5)\quad (K_2) = \frac{[(\mathbf{PNP})\mathbf{Ru{-}CO_2}]}{[(^*\mathbf{PNP})\mathbf{Ru}]\cdot \mathrm{pCO_2}}$$

From the equilibrium constants, the free energy changes can be obtained. To note, the equilibria that are concentration dependent will also have a concentration-dependent free energy (eq 6; standard-conditions are 1 M and 1 atm).

$$(6a)\quad \Delta G_{1,X} = -\mathrm{RT}\cdot\ln\left(\frac{[(\mathrm{PNP})\mathrm{Ru{-}X}]}{[(^*\mathbf{PNP})\mathbf{Ru}]\cdot[\mathrm{H{-}X}]^o}\cdot[\mathrm{H{-}X}]\right)$$

$$= \Delta G^o_{1,X} - \mathrm{RT}\cdot\ln\left([\mathrm{H{-}X}]\right)$$

$$(6b)\quad \Delta G_{1,H} = -\mathrm{RT}\cdot\ln\left(\frac{[(\mathrm{PNP})\mathrm{Ru{-}H}]}{[(^*\mathbf{PNP})\mathbf{Ru}]\cdot \mathrm{p^oH_2}}\cdot \mathrm{pH_2}\right)$$

$$= \Delta G^o_{1,H} - \mathrm{RT}\cdot\ln\left(\mathrm{pH_2}\right)$$

Table 1. Equilibrium constants and free energy change associated with coordination of H-X and CO_2 to **(*PNP)Ru**.

H-X	$\Delta G^o_{1,X}$ (kcal·mol^{-1})	$\Delta H^o_{1,X}$ (kcal·mol^{-1})	$\Delta S^o_{1,X}$ (cal·mol^{-1}·K^{-1})	$K_{1,X}$		
				293 K (1 atm, 1 M)	428 K (1 atm, 1 M)	428 K (50 bar, 1 mM)
H-H	-4.1 ± 0.2[h]	-17.4 ± 0.2	-45 ± 0.5	1100 ± 1.4[a,d,g]	0.13[a,d]	6.6[a,d]
(DMA-H)(DMC)	-0.03 ± 2[f,h]	-12.6 ± 1.5[f]	-42 ± 5[f]	1.3 ± 0.2	N.A.[e]	N.A.[e]
H-OCHO	-3.5 ± 0.2[h]	0.06 ± 0.15	12 ± 0.5	355 ± 38[b]	370[b,d]	0.37[b,d]
H-OMe	-2.0 ± 1.9[h]	-3.5 ± 1.3	-5.2 ± 4.6	25 ± 5[b]	4.6[b,d]	4.6×10^{-3} [b,d]
H-OH	-2.0 ± 0.6[h]	-0.6 ± 0.4	8.7 ± 1.4	5.4 ± 0.5[b]	41[b,d]	4.1×10^{-2} [b,d]
CO_2[c]	-3.8 ± 0.8[c,h]	-13.5 ± 0.6[c]	-33 ± 2[c]	633 ± 4[a,c,d,g]	0.55 [a,c,d]	27.6 [a,c,d]

[a] Units of atm^{-1}. [b] Units of M^{-1}. [c] Equilibrium with CO_2 corresponds to K_2. [d] Extrapolated from temperature-dependent data. [e] Not applicable, due to limited stability of DMC-H and (DMA-H)(DMC) at elevated temperatures. See text for details. [f] Energies obtained from a limited temperature-range (20-50 °C). [g] Error from propagation of the error of ΔG^o, $\sigma_K = \exp\left(\sigma_{\Delta G}/RT\right)$. [h] Error from propagation of the error of ΔH^o and ΔS^o, $\sigma_{\Delta G} = \sqrt{(\sigma_{\Delta H})^2 + (|T|\sigma_{\Delta S})^2}$. Error on the entropy and enthalpy are from the error in intercept and slope, respectively.

The free energy for the equilibrium with CO_2 is analogous to that for H_2 given in eq 6b. Thus, under non-standard states, the equilibrium constant is given by eq 7.

$$(7)\quad K_{1,X} = [\mathrm{H{-}X}]\exp\left(\frac{-\Delta G^o_{1,X}}{\mathrm{RT}}\right)$$

From equations 6 and 7, increasing the concentration of H-X at equilibrium will favor formation of **(PNP)Ru-X**. Equilibrium constants and equilibrium energies are given in Table 1.

The data in Table 1 indicate that under standard conditions, the reaction of **(*PNP)Ru** with H_2 is most favorable, followed by that with CO_2 and formic acid; that with (DMA-H)(DMC) and H_2O are least favored. These findings are consistent with the notion that if **(PNP)Ru-CO$_2$** is an off-cycle species, it can form competitively.[2c] Upon dilution, the equilibrium constants decrease accordingly for all H-X, with the exception of (DMA-H)(DMC). To our knowledge, only one other report considers equilibria with a dearomatized Ru species.[28] The study considered the reaction of various Lewis acids in the related PNN system, all of which bind akin to CO_2. While different equilibrium constants were obtained, concentration-dependence is not provided.

The free energy associated with addition of H_2 is similar to that observed by others whereby H_2 adds to give a metal dihydride.[29] It is smaller by ~ 2 kcal/mol than that found for a series of (P_2N_2)Ni species,[30] whereby H_2 is heterolytically cleaved, protonating the ligand with hydride attack at the Ni.

Given that catalysis ensues at elevated temperatures, the temperature-dependence of the equilibria was also determined. An overlay of the van't Hoff plots is shown in Figure 5 and the enthalpy and entropy are given in Table 1. During these studies, we found that **(PNP)Ru-OMe** and **(PNP)Ru-OH** are not stable at elevated temperatures, and hence a shifted temperature range was employed (see Figures S30-31).

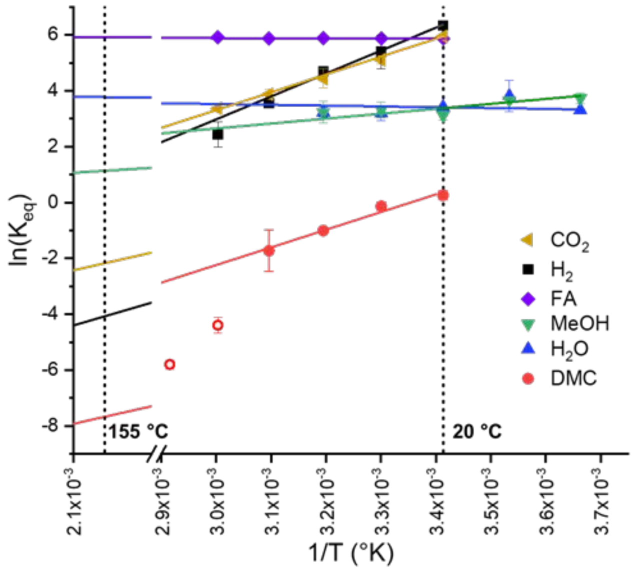

Figure 5. Overlay of van't Hoff plots for **(*PNP)Ru** + H-X or CO_2 in THF. Extrapolation shows the relative $K_{1,X}$ and K_2 at catalytic temperatures. K_{eq} has units of: M^{-1} for formic acid, water, MeOH; atm^{-1} for H_2, CO_2; unitless for (DMA-H)(DMC). For the equilibrium with (DMA-H)(DMC), the two points that are not filled are not included in the fit.

We also note that upon heating **(PNP)Ru-DMC** in the absence of DMA or (DMA-H)(DMC), some **(PNP)Ru-CO$_2$** forms that remains present upon cooling (see Figures S44-S45). This indicates that the free (DMC-H) is prone to release of CO_2, complicating equilibrium measurements at elevated temperatures (see SI). Indeed, the van't Hoff plot shown in Figure 5 shows a digression from linearity at 60 °C, which coincides with the temperature at which (DMA-H)(DMC) decomposes to DMA and CO_2.[31] We thus limit our analysis of the plot to temperatures less than 60 °C to extrapolate the enthalpy and entropy.

Figure 5 indicates that the relative equilibrium constants vary with temperature. At the temperature of catalysis, 155 °C, the equilibria with H_2 is least favored, followed by that with CO_2. This is notable as these are the most pertinent to catalysis. We note that through extrapolation, formation of **(PNP)Ru-DMC** is also expected to be unfavored at catalytic temperatures, though this equilibrium may not be pertinent at elevated temperatures (*vide supra*). Rather, formation of **(PNP)Ru-OCHO**, **(PNP)Ru-OH**, and **(PNP)Ru-OMe** are all favored. These represent equilibria with product species.

To favor binding of H_2 to give **(PNP)Ru-H** at elevated temperatures, higher pressures of H_2 can be used. Increasing the pressure to 50 bar (as in catalysis, *vide infra*) results in a factor of ~ 50 change in the equilibrium constant (Table 1). Non-standard conditions, whereby the concentration of H-X is less than 1 M, give lower equilibrium constants. This suggests that catalyst inhibition will indeed increase as product concentrations rise, regardless of the catalyst loading.

The equilibrium enthalpies appear to fall into two categories. For **(PNP)Ru-CO$_2$**, **(PNP)Ru-H**, and **(PNP)Ru-DMC**, the enthalpies are significant (< -12 kcal/mol), whilst for all others, they are modest (> -4 kcal/mol). In all instances, proton-transfer to the ligand ensues, so the difference in enthalpies must be attributed to the formation of strong Ru-X bonds and breaking of (relatively) weak bonds (*vide infra*). The three species that have the least negative enthalpies, **(PNP)Ru-OH**, **(PNP)Ru-OCHO**, and **(PNP)Ru-OMe**, are all produced from reaction with Brønsted acids. Ion-pairing and hydrogen-bonding may lead to a dissolution enthalpy and hence the larger (less negative) enthalpies. While **(PNP)Ru-DMC** should fall in this category as well, the discrepancy may be attributed to concomitant formation of DMA.

The large and negative entropy for **(PNP)Ru-CO$_2$** and **(PNP)Ru-H** is consistent with adding rigidity to the linear gas molecules. The entropy associated with **(PNP)Ru-DMC** of -42 $cal{\cdot}mol^{-1}{\cdot}K^{-1}$ suggests significant ordering upon its formation. Because these equilibria take two molecules to one, we anticipate large and negative entropies. However, this is not the case for formic acid, MeOH, and H_2O. This may indicate significant solvent ordering in the free H-X, or homoconjugation.[32] Formic acid, MeOH, and H_2O can all hydrogen-bond, and these interactions may in part increase the entropic contributions in THF.

p*K*$_a$ Measurements. In reactions that transfer net H_2 to or from a substrate, the H_2 is delivered as a hydride and a proton. This prompted us to investigate the pK_a of **(PNP)Ru$^+$**, (Figure 2, K_3) which is produced upon hydride transfer from **(PNP)Ru-H** to a substrate. Subsequent proton transfer then closes the catalytic cycle to give **(*PNP)Ru**. Moreover, knowledge of this pK_a, combined with the equilibrium with H_2, allows the hydricity of **(PNP)Ru-H** to be determined.[21]

Initial attempts to probe the pK_a of **(PNP)Ru$^+$** were hampered by coordination of the base to the Ru. The cationic 16-electron species has a vacant coordination site and allows for this. For instance, addition of TBMP (TBMP = 2,6-di-tert-butyl-4-methylpyridine) instead gave coordination of the base. This is evident by NMR spectroscopy, whereby the ^1H and ^{31}P resonances for **(PNP)Ru$^+$** shift, and no resonances ascribed to **(*PNP)Ru** are observed (see Figure S28). In some instances, treatment with the base gave **(*PNP)Ru** as the kinetic product, but over the course of hours, partially converts to the base-coordinated thermodynamic product. This is the case with (Li)(NMe_2), which converts to **(*PNP)Ru** prior to further reacting to give a species that is consistent with **(PNP)Ru-NMe$_2$** (see Figure S30).

To circumvent this, we turned to the non-nucleophilic phosphazene bases and their conjugate acids. Upon titration of (BTPPH)(BF_4) (pK_a = 20.2 in THF;[33] BTPP = *tert*-butylimino-tri(pyrrolidino)phosphorane) to a THF solution of **(*PNP)Ru**, **(PNP)Ru$^+$** is cleanly generated, as confirmed by NMR and UV-vis spectroscopies. Monitoring the titrations by UV-vis spectroscopy allows for the pK_a of 20.7 ± 0.2 to be determined (Figure 2, K_3). By contrast, the pK_a of the ligand, PNP, was found to be 28.6 ± 0.1 (see SI), similar to that estimated by others.[34] Thus, the ability for the anionic nitrogen to interact strongly with a metal renders the ligand more acidic by about 8 pK_a units.

We are also interested in establishing the effect that coordinating a 6th ligand has on the pK_a. This would allow for a suitable base to be used to bias the system and more favorably release X^- during catalysis. The ability to isolate both **[K][(*PNP)Ru-CO$_2$]** and **(PNP)Ru-CO$_2$** allows for such a comparison to be made (Figure 2, K_4). Titration of **[K][(*PNP)Ru-CO$_2$]** with (P_2EtH)(BF_4) gives a pK_a of 24.6 ± 0.4 (P_2Et = tetramethyl(tris(dimethylamino)phosphoranylidene)phosphorictriamide-Et-imin; pK_a = 25.3 in THF[33]). Coordination of a 6th ligand increases the ligand basicity by ~ 4 pK_a units. Together, these pK_a measurements indicate that the Ru center can greatly modulate the acidity of the ligand.

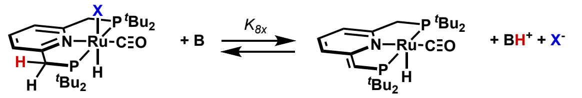

(8)

Titration of other **(PNP)Ru-X** (X = Cl, DMC, OCHO) species with a suitable base cleanly generates **(*PNP)Ru** (eq 8, K_{8x}). This equilibrium is formally a proton transfer followed by ligand loss and thus cannot give a true pK_a. (Scheme 2). However, knowledge of the pK_a for the added base (K_{BH+}) and estimation of K_{7x} allows for a lower-limit to the pK_a of **(PNP)Ru-X** to be obtained.

Scheme 2. Relationship between the equilibrium of eq 8 and the pK_a of **(PNP)Ru-X**.

$$\begin{array}{ll}
(\mathbf{PNP})\mathbf{Ru{-}X} \rightleftharpoons [(^*\mathbf{PNP})\mathbf{Ru{-}X}]^- + \mathrm{H}^+ & K_{5x} \\
[(^*\mathbf{PNP})\mathbf{Ru{-}X}]^- \rightleftharpoons (^*\mathbf{PNP})\mathbf{Ru} + \mathrm{X}^- & K_{7x} \\
\mathrm{B} + \mathrm{H}^+ \rightleftharpoons \mathrm{BH}^+ & (K_{BH+})^{-1} \\
\hline
(\mathbf{PNP})\mathbf{Ru{-}X} + \mathbf{B} \rightleftharpoons (^*\mathbf{PNP})\mathbf{Ru} + \mathrm{BH}^+ + X^- & K_{8x}
\end{array}$$

Ligand loss from **[(*PNP)Ru-X]$^-$** to **(*PNP)Ru** (K_{7x}) is expected to be favorable as the electron count drops from 20 to 18 (Figure 2). To probe this, 1 – 10 equivalents of ($^nBu_4N$)(X) (X = Cl or OCHO) were added to a 8.4 mM d_8-THF solution of **(*PNP)Ru**. No immediate change was observed by NMR spectroscopy (Figure S40), but for the chloride sample, **(PNP)Ru-Cl** is produced over the course of hours. This transformation necessitates a proton and likely occurs from Hofmann degradation[35] of the tetrabutylammonium cation, facilitating binding of the chloride. Addition of 10 equiv (Li)(DMC) to **(*PNP)Ru** gave no reaction (see Figure S43). As dimethylcarbamate is more basic than formate or chloride and hence should bind most favorably to the Ru, we assume that there is no appreciable reaction of the X^- species binding to **(*PNP)Ru**. Given the limits of what we can observe, we assign a lower limit of 100 to K_{7x}. The equilibrium constant is likely to be much larger, the extent of which will vary with the identity of X^- (*vide infra*).

This analysis provides lower-limits of 25 and 32 for the respective pK_a of **(PNP)Ru-OCHO** and **(PNP)Ru-DMC**. Shifting from a carboxylate to a chloride, **(PNP)Ru-Cl** further increases the basicity of the ligand, with a lower limit of the pK_a now being 34 (Table 2).

Table 2. Summary of pK_as and thermodynamic parameters pertinent to X^- release from **(PNP)Ru-X**.

Species	pK_a[a]	K_{6X} (M)[a]	$\Delta G^o_{6,X}$ (kcal·mol^{-1})
(PNP)	28.6 ± 0.1	--	--
(PNP)Ru$^+$	20.7 ± 0.2	--	--
(PNP)Ru-CO$_2$	24.6 ± 0.4	--	--
(PNP)Ru-OCHO	> 25	2 × 10^{-3}	3.7 ± 0.7
(PNP)Ru-DMC	> 32	9.6 × 10^{-11}	13.7 ± 0.7
(PNP)Ru-Cl	> 34	6.3 × 10^{-12}	15.3 ± 0.5
(PNP)Ru-H	--	5.0 × 10^{-32}	42.7 ± 0.6

[a]Measurements done at 20 °C. We assume that the equilibrium at 25 °C is ~ that at 20 °C.

Hydricity and binding constants. The hydricity of (PNP)Ru-H can be determined from the equilibria shown in Scheme 3.

Scheme 3. Equilibria employed to determine the hydricity of **(PNP)Ru-H**.

$$\begin{array}{ll}
(\mathbf{PNP})\mathbf{Ru{-}H} \rightleftharpoons (^*\mathbf{PNP})\mathbf{Ru} + \mathrm{H}_2 & (K_{1,H})^{-1} \\
(^*\mathbf{PNP})\mathbf{Ru} + \mathrm{H}^+ \rightleftharpoons (\mathbf{PNP})\mathbf{Ru}^+ & K_3 \\
\mathrm{H}_2 \rightleftharpoons \mathrm{H}^+ + \mathrm{H}^- & K_{\mathrm{H2-}} \\
\hline
(\mathbf{PNP})\mathbf{Ru{-}H} \rightleftharpoons (\mathbf{PNP})\mathbf{Ru}^+ + \mathrm{H}^- & K_{6,\mathrm{H}}
\end{array}$$

The hydricity is obtained by combining the pK_a of **(PNP)Ru$^+$**, the free energy of hydride transfer from H_2,[36,37] and the free energy of H_2 loss from **(PNP)Ru-H**. The thermochemical cycle gives a hydricity of 42.7 ± 0.6 kcal/mol (44.6 ± 0.6 kcal/mol using the value of K_{H2-} given in ref. 37) It is difficult to draw comparisons to the hydricity of other metal complexes, as this is the first reported hydricity in THF. As noted by others, hydricity values for metal complexes are solvent dependent,[38] with no qualitative trends that convert hydricity amongst solvents. This is also the first hydricity value reported for a metal complex that undergoes MLC; others have measured hydricities for P_2N_2-ligated metal hydrides,[30a,39] whereby protonation also occurs at the ligand, but subsequent proton transfer does not impact the nature of the metal-ligand bonds.

The hydricity allows for evaluation of whether hydride transfer to a substrate, for example, CO_2, is favorable. For that to be the case, the hydricity of **(PNP)Ru-H** must be less than that of formate. While it may be tempting to approximate that the hydricity of formate in THF must be greater than 42.7 kcal/mol, this is not valid in this system because the resulting formate binds to the Ru and this energy needs to be accounted for (Scheme 4). This binding may give an apparent increase in hydricity for **(PNP)Ru-H**, which can differ based on subsequent binding of the hydride-transferred product (Scheme 4, left).

Scheme 4. Relationship between hydricity and binding of formate to **[(PNP)Ru]$^+$** (two vertical equilibria).

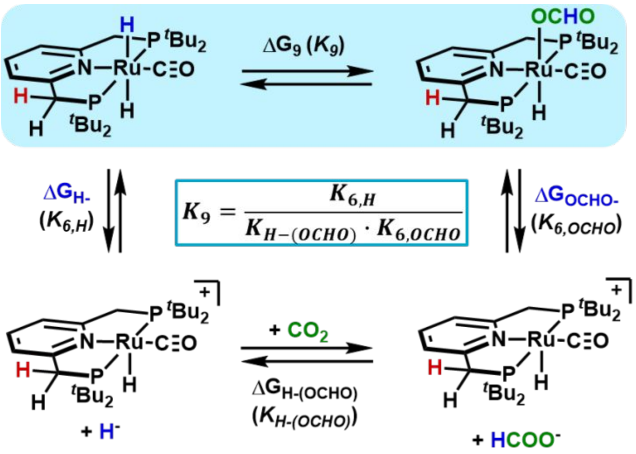

The free energy associated with release of formate from the Ru (Scheme 4, left) can be determined from one of the two thermochemical cycles, which are described in Scheme 5.

From this analysis, the free energy for formate release is 3.7 ± 0.7 kcal/mol (Table 2). This is appreciably less than the energy associated with DMC or chloride release, 13.7 and 15.3 kcal/mol respectively.

Binding of these species modifies the apparent hydricity. Formate binding gives an apparent hydricity of 39.0 kcal/mol (40.9 kcal/mol using the value of K_{H2-} given in ref. 37). Given that other X^- species bind more tightly, it is conceivable that the apparent hydricity can further be reduced. From this, and a lower-limit of 520 atm^{-1} for K_9 (Scheme 4 and Figure S24), we determine that the lower-limit for the hydricity of formate in THF is 42.7 kcal/mol (44.7 kcal/mol when using the values of ref. 37). For comparison, $\Delta G_{H\text{-}(OCHO)}$ is estimated to be 44 kcal/mol in MeCN, and 24.1 kcal/mol in water.[21]

The thermochemical cycles of Scheme 5 allow for the evaluation of the pK_as of H-OCHO and H-DMC in THF. Values of 20.8 ± 0.6 and 30.6 ± 0.6 are obtained, respectively. The value obtained for formic acid is similar to that of acetic acid in THF (22.5),[40] further validating our equilibration studies.

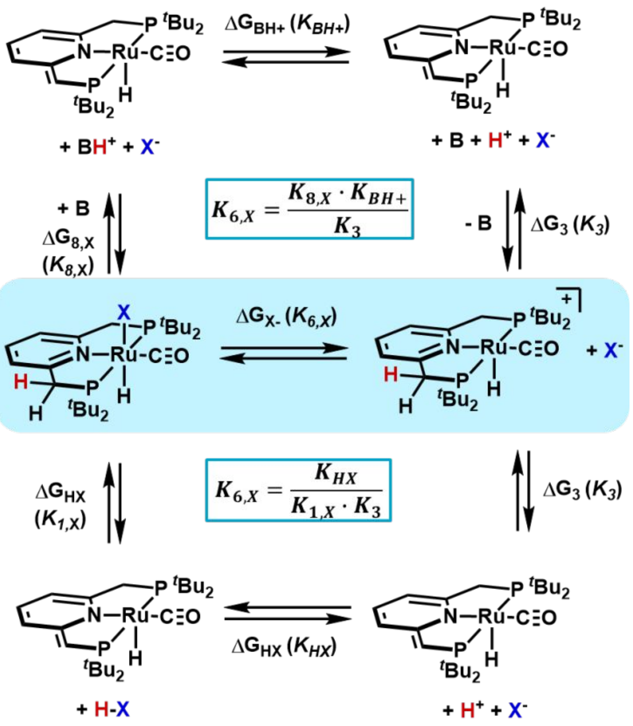

Scheme 5. Thermochemical cycles that can be employed to determine $K_{6,X}$ (highlighted in blue).

Catalytic Hydrogenation of CO$_2$. The hydrogenation of (DMA-H)(DMC) by **(PNP)Ru-Cl** was probed (Table 3). The use of dimethylammonium dimethylcarbamate as a CO$_2$ surrogate for hydrogenation to MeOH was first shown by Sanford by use of a related Ru catalyst.[7b] To draw comparisons, similar conditions were employed in terms of substrate and base equivalents, temperature, and solvent. We first examined the effect of catalyst concentration on conversion to MeOH, formate, and DMF, while maintaining a constant loading of 1 mol% (entries 1-5). As the catalyst concentration is increased from 0.05 mM to 5.3 mM, the TON of MeOH decreases. When the amount of MeOH produced is viewed instead as the concentration of MeOH, we see that except for 0.05 mM catalyst, the final concentration of MeOH is essentially constant (~2 mM). This suggests to us that there might be a deactivation mechanism that is dependent on the concentration of MeOH and/or H$_2$O. Indeed, during our equilibrium studies of **(*PNP)Ru** and MeOH/H$_2$O, we saw irreversible decomposition at elevated temperatures to intractable Ru species (See SI).

We then consider the effect of the base strength (entries 1, 6-9). Going from K$_3$PO$_4$ to ^{t}BuOK gives an increase in MeOH production. While the pK_as of K$_3$PO$_4$ and ^{t}BuOK are not known in THF, we note that the former is not capable of converting **(PNP)Ru-Cl** to **(*PNP)Ru** at room temperature, whilst the latter can, suggesting that ^{t}BuOK is more basic. When we use (Li)(DMC) as the base, we see an order of magnitude increase in TON to 39.4. Now, we reach our limiting concentration of MeOH produced with 0.05 mM catalyst loading. However, with (Li)(Me$_2$N) the TON drops to 1.6. We attribute this decrease to competitive amine binding which may occur at elevated temperatures. With **(^{Ph}P^{H}NP)Ru-(HBH$_3$)**, which is known to hydrogenate carbamates to MeOH,[7a,7b] we see no effect on varying the base (^{t}BuOK vs. K_3PO_4) on MeOH yield (see SI).

Given that the produced H_2O may quench one equiv of base, we also investigated using equimolar substrate and base. When we use equimolar ^{t}BuOK and (DMA-H)(DMC), we see a slight decrease in TON compared to when we use 1:2 base:substrate (Table S4). A decrease is also observed when we use 1:4 base:substrate. We interpret these results as suggesting an intricate balance between the requirement of the base, and the impact of adding base to the equilibrium of (DMA-H)(DMC) and DMA + CO_2 (with base favoring formation of DMC salts).

To determine if there is a substrate which is limiting TON, we compared the substrate (entries 1, 10-12). Going from (DMA-H)(DMC) to (Li)(DMC), we see a doubling of the MeOH TON. This may be due to lower concentrations of amine (DMA-H$^+$ versus Li$^+$) or discrepancies in how readily CO_2 is released from DMC. Formic acid is poorly hydrogenated, which may be due to the now acidic nature of the reaction medium, as only 50 equivalents of base was added. When DMF is employed as a substrate, we see MeOH produced with a TON of 59.2, again giving a similar limiting final concentration.

Table 3. Hydrogenation of (DMA-H)(DMC) by **(PNP)Ru-Cl**. All reactions are run in 10 mL THF.

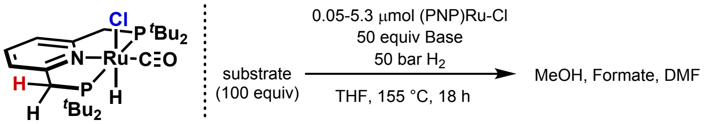

Entry	[catalyst] (mM) (mol%)	Substrate	Base	TON MeOH (mM)[a]	TON Formate (mM)[b]	TON DMF (mM)[a]
1	0.05 (1%)	(DMA-H)(DMC)[g]	^{t}BuOK	3.9 ± 0.3 (0.20)	3.3 ± 0.2 (0.17)	19.8 ± 5.4 (4.1)
2	0.5 (1%)	(DMA-H)(DMC)[g]	^{t}BuOK	4.0 ± 0.2 (2.1)	5.3 ± 0.2 (2.6)	57.2 ± 15.8 (140)
3	1.5 (1%)	(DMA-H)(DMC)[g]	^{t}BuOK	1.2 ± 0.2 (1.7)	0.6 ± 0.1 (0.90)	0.5 ± 0.3 (57)
4	3.3 (1%)	(DMA-H)(DMC)[g]	^{t}BuOK	0.5 ± 0.1 (1.7)	0.3 ± 0.1 (0.98)	n.d.[e]
5	5.3 (1%)	(DMA-H)(DMC)[g]	^{t}BuOK	0.4 ± 0.1 (2.0)	0.8 ± 0.1 (4.5)	0.3 ± 0.3 (0.016)
6[c]	0.05 (1%)	(DMA-H)(DMC)[g]	None	2.0 ± 0.7 (0.065)	0.7 ± 0.4 (0.046)	n.d.[e]
7	0.05 (1%)	(DMA-H)(DMC)[g]	K_3PO_4	2.6 ± 0.5 (0.14)	1.6 ± 0.7 (0.23)	10.9 ± 7.7 (4.1)
8	0.05 (1%)	(DMA-H)(DMC)[g]	(Li)(DMC)[d]	39.4 ± 0.4 (2.0)	6.3 ± 5.7 (0.32)	0.5 ± 0.4 (0.00095)
9	0.05 (1%)	(DMA-H)(DMC)[g]	(Li)(Me_2N)	1.6 ± 0.3 (0.078)	0.7 ± 0.4 (0.035)	1.0 ± 1.0 (0.001)

10	0.05 (1%)	(Li)(DMC)	None	7.5 ± 4.9 (0.38)	1.3 ± 0.5 (0.065)	n.d.[e]
11	0.05 (1%)	HCOOH	^tBuOK	1.2 ± 0.6 (0.062)	--[f]	n.d.[e]
12	0.05 (1%)	DMF	^tBuOK	59.2 ± 2.3 (2.9)	0.7 ± 0.3 (3.6×10^{-5})	--[f]

[a]Quantified by GC. Error from duplicate catalytic runs. [b]Quantified by IC. Error from duplicate catalytic runs. [c]**(*PNP)Ru** used as the catalyst. [d]100 equiv of base employed. [e]n.d. = not detected. [f]not quantified. [g]92 equiv of substrate employed.

DISCUSSION

Ramifications of H-X equilibria on catalysis. Given the concentration (or pressure) dependence for the equilibria of **(*PNP)Ru** and H-X or CO_2, it is imperative to understand how different catalyst loadings impact TON. Regardless of the catalyst concentration, only the H-X concentration will determine the equilibrium position. This is illustrated when considering the TON of MeOH produced. While varying the catalyst loading impacts the TON for MeOH, at the four highest loadings considered it did not impact the overall concentration of MeOH produced, ~ 2 mM. This same concentration can be obtained at lower catalyst loading when using (Li)(DMC) as the base. Strikingly, when DMF is instead used as a substrate, the same concentration of MeOH is produced. This suggests that competitive equilibria may limit the overall MeOH production. Indeed, at elevated temperatures, the equilibrium to give **(PNP)Ru-OMe** is favored over that of **(PNP)Ru-H**. In this system, further complication likely arises from the instability of **(*PNP)Ru** to excess MeOH at elevated temperatures; the ability for the catalyst to turnover suggests that this deactivating equilibrium is less favorable than that which gives productive turnover.

A threshold MeOH concentration is not unique to our system. Both Sanford and Prakash have used **($^{Ph}P^{H}NP$)Ru-Cl** and **($^{Ph}P^{H}NP$)Ru-(HBH_3)** to hydrogenate CO_2 to MeOH in the presence of a variety of amines. Under their conditions, Sanford reports a maximum MeOH concentration of about 1 M.[7b] In three separate reports, Prakash reports maximum MeOH concentrations of 1.3 M,[14] and 2.1 M.[7a,41] That the same catalyst, run under different conditions, in different solvents, amines, and base additives, all give a similar maximum MeOH concentration suggests a concentration-dependent equilibrium between MeOH and the catalyst contributes to catalyst performance. Related Ru catalysts that undergo MLC via dearomatization give ~1 M limiting MeOH concentrations in other types of hydrogenations.[7c,26b] The discrepancy between the catalysts likely has contributions from differences in equilibrium constants, and in the latter systems, different H-X species present and hence different competing equilibria. Regardless, these similarities suggest that a better parameter for evaluating catalysis is product concentration, not TON.

Knowing both the concentration and temperature-dependence of these equilibria ($K_{1,X}$) allows for a better understanding of how to optimize reaction conditions. In general, the equilibrium constant towards **(PNP)Ru-X** decreases with temperature, and the substrates fall into two classes that differ by the magnitude of this effect. Our study shows that the decrease is not uniform across all substrates. Thus, the equilibrium with formic acid is more or less temperature independent, whilst that with H_2 shows a strong decrease with increasing temperatures. If formation of **(PNP)Ru-OCHO** does indeed represent a thermodynamic bottleneck, or the most favorable equilibrium, then increasing the temperature would not favor formation of **(PNP)Ru-H**; only raising the pressure or lowering the temperature would do so. Varying the temperature and concentrations can likewise impact the thermodynamic bottlenecks; the extent of which would not be known without studies such as this.

These findings are not unique to hydrogenation of carbamates to MeOH. For example, using **($^{Ph}P^{H}NP$)Ru(HBH_3)**, the optimal temperature for CO_2 hydrogenation to DMF (in the presence of DMA) is found to be 95 °C,[7b] well below the 155 °C used to hydrogenate the produced DMF to MeOH. This is consistent with the idea of the relative equilibria shifting with temperature. Also, a recent study on dehydrogenative coupling of ethylenediamine and MeOH to give ethylene urea and H_2 showed that increasing the headspace volume, effectively decreasing the [H_2], enhances this Ru catalyzed reaction.[42] These studies on related Ru catalysts that undergo MLC reinforce the need to understand the thermodynamic parameters associated with the catalyst; this allows for optimization of the catalytic conditions.

Knowledge of the temperature and pressure dependence for the H_2 equilibrium versus that with CO_2 is also pertinent to CO_2 hydrogenation. With regards to hydrogenation to formate, Pidko has suggested that (**(PNP)Ru-CO_2**) is an inhibitive, off-cycle species[2c] and Sanford suggests that the related (**(PNN)Ru-CO_2**) may be able to do catalysis, albeit at a slower rate;[2a] this species should therefore be minimized under catalytic conditions. Our studies indicate that at all elevated temperatures, the equilibrium with CO_2 is favored over that of H_2 and thus pressure differences must be employed. While this is usually achieved by changing the partial pressures of the two gases, it can also be achieved by using "captured CO_2" in the form of carbamates and carbamic acid. These are in equilibria with free CO_2 (eq 9).

$$□□□CO_2 + R_2NH \rightleftarrows R_2N^+(H)(COO^-) \rightleftarrows R_2N-COOH \xrightleftharpoons{R_2'NH} [R_2N-COO][R_2'NH_2]$$

Moreover, it has been shown that by changing the amine identity or using mixtures of amines, the pressure and temperature requirements for releasing CO_2 can be greatly modified.[43] This relative equilibria is particularly pertinent to carbon capture and recycling schemes, as CO_2 release is energy-intensive. Coupling release to catalysis will streamline the process, and by judicious choice of amine, will allow for tailoring the H_2:CO_2 to optimize catalysis.

Rationalization of the need for a strong base during catalysis. It is established that using **(PNP)Ru-Cl** with DBU as a co-substrate base allows for CO_2 hydrogenation to formate.[2d,20] While DBU, having a pK_a of 16.1 in THF,[40] is not sufficiently basic enough to deprotonate **(PNP)Ru-OCHO** at room temperature, precipitation of (DBU-H)(OCHO) is not accounted for, nor are subsequent equilibria with the product **(*PNP)Ru**, both of which could drive the reaction. It is thus conceivable that under reaction conditions, which include elevated temperatures, this deprotonation readily occurs. Indeed, treatment of **(PNP)Ru-Cl** with K_3PO_4 at room temperature gives no reaction, but upon warming to 120 °C, formation of (***PNP)Ru** ensues, as evident by the characteristic color change from yellow to green. Cooling the sample causes it to revert back to **(PNP)Ru-Cl**. There is thus a temperature dependence on the pK_a, but deconvoluting the contribution of the inorganic base and the Ru species is not trivial.

Our results suggest that using a stronger base allows for and increases MeOH production when **(PNP)Ru-Cl** is used as a catalyst for the hydrogenation of (DMA-H)(DMC). Given the amount of base added, we cannot conclude whether it is a co-reagent or a co-catalyst. Others have noted that in related hydrogenations, addition of a base enhances catalysis, though the base is added in sub-stoichiometric amounts.[7b,14] It is speculated that the base enhances the MLC mechanism, and thus the base strength may alter the mechanism.

As noted by others, K_3PO_4 is sufficient for MeOH production when **($^{Ph}P^{H}$NP)Ru(HBH_3)** is used as the catalyst for hydrogenation of (DMA-H)(DMC).[7a] Changing the base to KO^{t}Bu does not improve MeOH production. By contrast, with **(PNP)Ru-X** a stronger base is required. This suggests that the base is used to deprotonate the catalyst. The alternative, deprotonation of an organic intermediate, would show the same base-dependence, regardless of the catalyst.

This can be rationalized by considering our pK_a measurements, which indicate that 6-coordinate **(PNP)Ru-X** species are at least 5 pK_a units more basic than 5-coordinate **(PNP)Ru$^+$**. Thus, addition of a strong base can bias the system to regenerate (***PNP)Ru**. It should be noted that of the 6-coordinate **(PNP)Ru-X** species whose pK_a we could estimate, **(PNP)Ru-OCHO** gave the lowest value, consistent with a relatively weak base (DBU) facilitating this hydrogenation. Additionally, our equilibrium studies indicate that **(PNP)Ru-OCHO** does not readily dissociate formic acid, even at elevated temperatures. This suggests that the only way to turn over the catalyst is to use a base. Our best results for MeOH production used (Li)(DMC) as the base. From our thermochemical cycles, the pK_a of DMC-H, dimethylcarbamic acid, is 30.6, significantly higher than the DBU that is needed for formate. It therefore may serve to deprotonate a **(PNP)Ru-X** species that is pertinent to DMF hydrogenation.

Hydricity is modified by binding of substrate. Miller and coworkers recently disclosed how hydricity of Ru and Ir hydrides varies in H_2O with added buffers that can coordinate to the metal.[44] In their work, they found that binding of H_2O versus Cl^- can alter the apparent hydricity by about 3-5 kcal/mol. While their studies focused on buffers, here we extend this idea to how coordination of the product of hydride transfer impacts the apparent hydricity.

Our analysis gives a hydricity of 42.7 kcal/mol for **(PNP)Ru-H** in THF. This is the value to consider if the substrate does not coordinate to the Ru as part of the catalytic cycle. However, our thermodynamic studies indicate that substrate binding is favorable, giving **(PNP)Ru-X**. This binding is favorable by ~4-15 kcal/mol, and hence can greatly impact the apparent hydricity. If hydrogenation does occur via coordination of the product of hydride transfer, for example, formate, then catalyst hydricity does not need to be great er than that of formate. Rather, the catalyst hydricity and binding affinity for the product must be larger than that of formate. Due to the inability to isolate **(PNP)Ru-OMe**, we are unable to determine the methoxide binding affinity. However, Table 2 suggests that it may differ from that of formate and require different hydricity parameters from the catalyst.

CONCLUSIONS

We presented a thorough thermochemical analysis of the Ru PNP hydrogenation catalyst. The temperature-dependent equilibrium studies suggest what may be thermodynamic bottlenecks and how they vary with temperature. At elevated temperatures, **(PNP)Ru-OCHO** formation is favored over **(PNP)Ru-H** by 4 orders of magnitude in $K_{1,X}$. This explains why formic acid is not readily released, but rather a base is required to convert **(PNP)Ru-OCHO** to **(*PNP)Ru**. A stronger base is required in this system to drive hydrogenation of (DMA-H)(DMC) to MeOH, while this is not a requirement in related systems. We find that the pK_a of **(PNP)Ru-X** varies greatly with the identity of the X-ligand, and hence suggest that the stronger base is required to deprotonate a 6-coordinate Ru species that is bound by an intermediate *en route* to MeOH production. Our hydrogenation studies indicate that there is a limiting methanol concentration that is reached with this system. While there are likely many factors to this, the equilibria studies are consistent with this observation and likely contributes to performance. We also give a lower estimate for the hydricity of formate in THF, and indicate how substrate binding can impact the apparent hydricity of a catalyst by several kcal/mol. This work mirrors that done in the electrochemical field, whereby such findings have allowed for better H_2 evolution catalysts to be developed and have helped ascertain catalyst requirements for electrocatalytic CO_2 reduction.[15-16] Although this work benchmarks several thermochemical properties pertinent to CO_2 hydrogenation catalysts, we envision that our findings will be broadly applicable to a variety of other catalytic reactions performed by this and related catalysts that require cooperation between the metal and bifunctional ligand.

ASSOCIATED CONTENT

Supporting Information

The Supporting Information is available free of charge on the ACS Publications website.

Experimental details, including syntheses, NMR and UV-vis data, and equilibrium plots (PDF)

Crystallographic data (CIF)

AUTHOR INFORMATION

Corresponding Author

*caroline.saouma@utah.edu

Notes

The authors declare no competing financial interest.

ACKNOWLEDGMENT

The authors gratefully acknowledge start-up funding from the University of Utah and USTAR, ACS PRF (57058-DNI3), and NSF REU (1659579).

REFERENCES

(1) (a) Khusnutdinova, J. R.; Milstein, D. Metal–Ligand Cooperation *Angew. Chem. Int. Ed.* **2015**, *54*, 12236; (b) Alig, L.; Fritz, M.; Schneider, S. First-Row Transition Metal (De)Hydrogenation Catalysis Based On Functional Pincer Ligands *Chem. Rev.* **2019**, *119*, 2681; (c) Gunanathan, C.; Milstein, D. Bond activation and catalysis by ruthenium pincer complexes *Chem. Rev.* **2014**, *114*, 12024.

(2) Examples with Ru: (a) Huff, C. A.; Sanford, M. S. Catalytic CO_2 Hydrogenation to Formate by a Ruthenium Pincer Complex *ACS Catal.* **2013**, *3*, 2412; (b) Filonenko, G. A.; Smykowski, D.; Szyja, B. M.; Li, G.; Szczygieł, J.; Hensen, E. J. M.; Pidko, E. A. Catalytic Hydrogenation of CO_2 to Formates by a Lutidine-Derived Ru–CNC Pincer Complex: Theoretical Insight into the Unrealized Potential *ACS Catal.* **2015**, *5*, 1145; (c) Filonenko, G. A.; Hensen, E. J. M.; Pidko, E. A. Mechanism of CO_2 hydrogenation to formates by homogeneous Ru-PNP pincer catalyst: from a theoretical description to performance optimization *Catal. Sci. Technol.* **2014**, *4*, 3474; (d) Filonenko, G. A.; Conley, M. P.; Copéret, C.; Lutz, M.; Hensen, E. J. M.; Pidko, E. A. The impact of Metal–Ligand Cooperation in Hydrogenation of Carbon Dioxide Catalyzed by Ruthenium PNP Pincer *ACS Catal.* **2013**, *3*, 2522.

(3) Examples with Ir: (a) Tanaka, R.; Yamashita, M.; Nozaki, K. Catalytic Hydrogenation of Carbon Dioxide Using Ir(III)–Pincer Complexes *J. Am. Chem. Soc.* **2009**, *131*, 14168; (b) Schmeier, T. J.; Dobereiner, G. E.; Crabtree, R. H.; Hazari, N. Secondary Coordination Sphere Interactions Facilitate the Insertion Step in an Iridium(III) CO_2 Reduction Catalyst *J. Am. Chem. Soc.* **2011**, *133*, 9274.

(4) Examples with 1st row transition metals: (a) Langer, R.; Diskin-Posner, Y.; Leitus, G.; Shimon, L. J. W.; Ben-David, Y.; Milstein, D. Low-Pressure Hydrogenation of Carbon Dioxide Catalyzed by an Iron Pincer Complex Exhibiting Noble Metal Activity *Angew. Chem. Int. Ed.* **2011**, *50*, 9948; (b) Bernskoetter, W. H.; Hazari, N. Reversible Hydrogenation of Carbon Dioxide to Formic Acid and Methanol: Lewis Acid Enhancement of Base Metal Catalysts *Acc. Chem. Res.* **2017**, *50*, 1049; (c) Bielinski, E. A.; Lagaditis, P. O.; Zhang, Y.; Mercado, B. Q.; Würtele, C.; Bernskoetter, W. H.; Hazari, N.; Schneider, S. Lewis Acid-Assisted Formic Acid Dehydrogenation Using a Pincer-Supported Iron Catalyst *J. Am. Chem. Soc.* **2014**, *136*, 10234; (d) Bertini, F.; Glatz, M.; Gorgas, N.; Stöger, B.; Peruzzini, M.; Veiros, L. F.; Kirchner, K.; Gonsalvi, L. Carbon dioxide hydrogenation catalysed by well-defined Mn(i) PNP pincer hydride complexes *Chem. Sci.* **2017**, *8*, 5024.

(5) Examples with Ru: Zhang, L.; Han, Z.; Zhao, X.; Wang, Z.; Ding, K. Highly Efficient Ruthenium-Catalyzed N-Formylation of Amines with H_2 and CO_2 *Angew. Chem. Int. Ed.* **2015**, *54*, 6186.

(6) Examples with 1st row transition metals: (a) Jayarathne, U.; Hazari, N.; Bernskoetter, W. H. Selective Iron-Catalyzed N-Formylation of Amines using Dihydrogen and Carbon Dioxide *ACS Catal.* **2018**, *8*, 1338; (b) Daw, P.; Chakraborty, S.; Leitus, G.; Diskin-Posner, Y.; Ben-David, Y.; Milstein, D. Selective N-Formylation of Amines with H_2 and CO_2 Catalyzed by Cobalt Pincer Complexes *ACS Catal.* **2017**, *7*, 2500.

(7) Examples with Ru: (a) Kothandaraman, J.; Goeppert, A.; Czaun, M.; Olah, G. A.; Prakash, G. K. S. Conversion of CO_2 from Air into Methanol Using a Polyamine and a Homogeneous Ruthenium Catalyst *J. Am. Chem. Soc.* **2016**, *138*, 778; (b) Rezayee, N. M.; Huff, C. A.; Sanford, M. S. Tandem Amine and Ruthenium-Catalyzed Hydrogenation of CO_2 to Methanol *J. Am. Chem. Soc.* **2015**, *137*, 1028; (c) Khusnutdinova, J. R.; Garg, J. A.; Milstein, D. Combining Low-Pressure CO_2 Capture and Hydrogenation To Form Methanol *ACS Catal.* **2015**, *5*, 2416; (d) Everett, M.; Wass, D. F. Highly productive CO_2 hydrogenation to methanol – a tandem catalytic approach via amide intermediates *Chem. Commun.* **2017**, *53*, 9502.

(8) Examples with 1st row transition metals: (a) Ribeiro, A. P. C.; Martins, L. M. D. R. S.; Pombeiro, A. J. L. Carbon dioxide-to-methanol single-pot conversion using a C-scorpionate iron(ii) catalyst *Green Chemistry* **2017**, *19*, 4811; (b) Kar, S.; Goeppert, A.; Kothandaraman, J.; Prakash, S. G. K. Manganese-Catalyzed Sequential Hydrogenation of CO_2 to Methanol via Formamide *ACS Catal.* **2017**, 6347.

(9) Wang, W.-H.; Himeda, Y.; Muckerman, J. T.; Manbeck, G. F.; Fujita, E. CO_2 Hydrogenation to Formate and Methanol as an Alternative to Photo- and Electrochemical CO_2 Reduction *Chem. Rev.* **2015**, *115*, 12936.

(10) Yang, X. Hydrogenation of Carbon Dioxide Catalyzed by PNP Pincer Iridium, Iron, and Cobalt Complexes: A Computational Design of Base Metal Catalysts *ACS Catal.* **2011**, *1*, 849.

(11) (a) Schneidewind, J.; Adam, R.; Baumann, W.; Jackstell, R.; Beller, M. Low-Temperature Hydrogenation of Carbon Dioxide to Methanol with a Homogeneous Cobalt Catalyst *Angew. Chem. Int. Ed.* **2017**, *56*, 1890; (b) Wesselbaum, S.; Moha, V.; Meuresch, M.; Brosinski, S.; Thenert, K. M.; Kothe, J.; Stein, T. v.; Englert, U.; Holscher, M.; Klankermayer, J.; Leitner, W. Hydrogenation of carbon dioxide to methanol using a homogeneous ruthenium-Triphos catalyst: from mechanistic investigations to multiphase catalysis *Chem. Sci.* **2015**, *6*, 693; (c) Wesselbaum, S.; vom Stein, T.; Klankermayer, J.; Leitner, W. Hydrogenation of Carbon Dioxide to Methanol by Using a Homogeneous Ruthenium–Phosphine Catalyst *Angew. Chem. Int. Ed.* **2012**, *51*, 7499; (d) Huff, C. A.; Sanford, M. S. Cascade Catalysis for the Homogeneous Hydrogenation of CO_2 to Methanol *J. Am. Chem. Soc.* **2011**, *133*, 18122.

(12) Vitillo, J. G.; Smit, B.; Gagliardi, L. Introduction: Carbon Capture and Separation *Chem. Rev.* **2017**, *117*, 9521.

(13) Heldebrant, D. J.; Koech, P. K.; Glezakou, V.-A.; Rousseau, R.; Malhotra, D.; Cantu, D. C. Water-Lean Solvents for Post-Combustion CO_2 Capture: Fundamentals, Uncertainties, Opportunities, and Outlook *Chem. Rev.* **2017**, *117*, 9594.

(14) Kar, S.; Sen, R.; Kothandaraman, J.; Goeppert, A.; Chowdhury, R.; Munoz, S. B.; Haiges, R.; Prakash, G. K. S. Mechanistic Insights into Ruthenium-Pincer-Catalyzed Amine-Assisted Homogeneous Hydrogenation of CO_2 to Methanol *J. Am. Chem. Soc.* **2019**, *141*, 3160.

(15) (a) DuBois, D. L. Development of Molecular Electrocatalysts for Energy Storage *Inorg. Chem.* **2014**, *53*, 3935; (b) Helm, M. L.; Stewart, M. P.; Bullock, R. M.; DuBois, M. R.; DuBois, D. L. A Synthetic Nickel Electrocatalyst with a Turnover Frequency Above 100,000

s^{-1} for H_2 Production *Science* **2011**, *333*, 863; (c) Sherbow, T. J.; Fettinger, J. C.; Berben, L. A. Control of Ligand pK_a Values Tunes the Electrocatalytic Dihydrogen Evolution Mechanism in a Redox-Active Aluminum(III) Complex *Inorg. Chem.* **2017**, *56*, 8651; (d) Rountree, E. S.; Martin, D. J.; McCarthy, B. D.; Dempsey, J. L. Linear Free Energy Relationships in the Hydrogen Evolution Reaction: Kinetic Analysis of a Cobaloxime Catalyst *ACS Catal.* **2016**, *6*, 3326.

(16) (a) Taheri, A.; Thompson, E. J.; Fettinger, J. C.; Berben, L. A. An Iron Electrocatalyst for Selective Reduction of CO_2 to Formate in Water: Including Thermochemical Insights *ACS Catal.* **2015**, *5*, 7140; (b) Waldie, K. M.; Ostericher, A. L.; Reineke, M. H.; Sasayama, A. F.; Kubiak, C. P. Hydricity of Transition-Metal Hydrides: Thermodynamic Considerations for CO_2 Reduction *ACS Catal.* **2018**, *8*, 1313.

(17) Jeletic, M. S.; Hulley, E. B.; Helm, M. L.; Mock, M. T.; Appel, A. M.; Wiedner, E. S.; Linehan, J. C. Understanding the Relationship Between Kinetics and Thermodynamics in CO_2 Hydrogenation Catalysis *ACS Catal.* **2017**, *7*, 6008.

(18) (a) Gnanaprakasam, B.; Zhang, J.; Milstein, D. Direct Synthesis of Imines from Alcohols and Amines with Liberation of H2 *Angew. Chem. Int. Ed.* **2010**, *49*, 1468; (b) Gnanaprakasam, B.; Balaraman, E.; Ben-David, Y.; Milstein, D. Synthesis of Peptides and Pyrazines from β-Amino Alcohols through Extrusion of H2 Catalyzed by Ruthenium Pincer Complexes: Ligand-Controlled Selectivity *Angew. Chem. Int. Ed.* **2011**, *50*, 12240; (c) Xie, Y.; Ben-David, Y.; Shimon, L. J. W.; Milstein, D. Highly Efficient Process for Production of Biofuel from Ethanol Catalyzed by Ruthenium Pincer Complexes *J. Am. Chem. Soc.* **2016**, *138*, 9077.

(19) (a) Zeng, R.; Feller, M.; Ben-David, Y.; Milstein, D. Hydrogenation and Hydrosilylation of Nitrous Oxide Homogeneously Catalyzed by a Metal Complex *J. Am. Chem. Soc.* **2017**, *139*, 5720; (b) Mukherjee, A.; Srimani, D.; Ben-David, Y.; Milstein, D. Low-Pressure Hydrogenation of Nitriles to Primary Amines Catalyzed by Ruthenium Pincer Complexes. Scope and mechanism *ChemCatChem* **2017**, *9*, 559.

(20) Li, Z.; Rayder, T. M.; Luo, L.; Byers, J. A.; Tsung, C.-K. Aperture-Opening Encapsulation of a Transition Metal Catalyst in a Metal–Organic Framework for CO_2 Hydrogenation *J. Am. Chem. Soc.* **2018**, *140*, 8082.

(21) Wiedner, E. S.; Chambers, M. B.; Pitman, C. L.; Bullock, R. M.; Miller, A. J. M.; Appel, A. M. Thermodynamic Hydricity of Transition Metal Hydrides *Chem. Rev.* **2016**, *116*, 8655.

(22) Bauer, J. O.; Leitus, G.; Ben-David, Y.; Milstein, D. Direct Synthesis of Symmetrical Azines from Alcohols and Hydrazine Catalyzed by a Ruthenium Pincer Complex: Effect of Hydrogen Bonding *ACS Catalysis* **2016**, *6*, 8415.

(23) Montag, M.; Zhang, J.; Milstein, D. Aldehyde Binding through Reversible C–C Coupling with the Pincer Ligand upon Alcohol Dehydrogenation by a PNP–Ruthenium Catalyst *J. Am. Chem. Soc.* **2012**, *134*, 10325.

(24) Vogt, M.; Gargir, M.; Iron, M. A.; Diskin-Posner, Y.; Ben-David, Y.; Milstein, D. A New Mode of Activation of CO_2 by Metal–Ligand Cooperation with Reversible C-C and M-O Bond Formation at Ambient Temperature *Chem. Eur. J.* **2012**, *18*, 9194.

(25) Kothandaraman, J.; Goeppert, A.; Czaun, M.; Olah, G. A.; Surya Prakash, G. K. CO_2 capture by amines in aqueous media and its subsequent conversion to formate with reusable ruthenium and iron catalysts *Green Chemistry* **2016**, *18*, 5831.

(26) For instability of related species with the PNN ligand, see: (a) Kohl, S. W.; Weiner, L.; Schwartsburd, L.; Konstantinovski, L.; Shimon, L. J. W.; Ben-David, Y.; Iron, M. A.; Milstein, D. Consecutive Thermal H_2 and Light-Induced O_2 Evolution from Water Promoted by a Metal Complex *Science* **2009**, *324*, 74; (b) Balaraman, E.; Gunanathan, C.; Zhang, J.; Shimon, L. J. W.; Milstein, D. Efficient hydrogenation of organic carbonates, carbamates and formates indicates alternative routes to methanol based on CO2 and CO *Nat Chem* **2011**, *3*, 609.

(27) Zhang, L.; Nguyen, D. H.; Raffa, G.; Trivelli, X.; Capet, F.; Desset, S.; Paul, S.; Dumeignil, F.; Gauvin, R. M. Catalytic Conversion of Alcohols into Carboxylic Acid Salts in Water: Scope, Recycling, and Mechanistic Insights *ChemSusChem* **2016**, *9*, 1413.

(28) Huff, C. A.; Kampf, J. W.; Sanford, M. S. Reversible carbon–carbon bond formation between carbonyl compounds and a ruthenium pincer complex *Chem. Commun.* **2013**, *49*, 7147.

(29) Lilio, A. M.; Reineke, M. H.; Moore, C. E.; Rheingold, A. L.; Takase, M. K.; Kubiak, C. P. Incorporation of Pendant Bases into Rh(diphosphine)$_2$ Complexes: Synthesis, Thermodynamic Studies, And Catalytic CO_2 Hydrogenation Activity of $[Rh(P_2N_2)_2]^+$ Complexes *J. Am. Chem. Soc.* **2015**, *137*, 8251.

(30) (a) Lense, S.; Ho, M.-H.; Chen, S.; Jain, A.; Raugei, S.; Linehan, J. C.; Roberts, J. A. S.; Appel, A. M.; Shaw, W. Incorporating Amino Acid Esters into Catalysts for Hydrogen Oxidation: Steric and Electronic Effects and the Role of Water as a Base *Organometallics* **2012**, *31*, 6719; (b) Wilson, A. D.; Newell, R. H.; McNevin, M. J.; Muckerman, J. T.; DuBois, M. R.; DuBois, D. L. Hydrogen oxidation and production using nickel-based molecular catalysts with positioned proton relays *J. Am. Chem. Soc.* **2006**, *128*, 358.

(31) Chen, L.; Guo, S.-X.; Li, F.; Bentley, C.; Horne, M.; Bond, A. M.; Zhang, J. Electrochemical Reduction of CO_2 at Metal Electrodes in a Distillable Ionic Liquid *ChemSusChem* **2016**, *9*, 1271.

(32) McCarthy, B. D.; Martin, D. J.; Rountree, E. S.; Ullman, A. C.; Dempsey, J. L. Electrochemical Reduction of Brønsted Acids by Glassy Carbon in Acetonitrile—Implications for Electrocatalytic Hydrogen Evolution *Inorg. Chem.* **2014**, *53*, 8350.

(33) Kaljurand, I.; Saame, J.; Rodima, T.; Koppel, I.; Koppel, I. A.; Kögel, J. F.; Sundermeyer, J.; Köhn, U.; Coles, M. P.; Leito, I. Experimental Basicities of Phosphazene, Guanidinophosphazene, and Proton Sponge Superbases in the Gas Phase and Solution *J. Phys. Chem. A* **2016**, *120*, 2591.

(34) Simler, T.; Karmazin, L.; Bailly, C.; Braunstein, P.; Danopoulos, A. A. Potassium and Lithium Complexes with Monodeprotonated, Dearomatized PNP and PNCNHC Pincer-Type Ligands *Organometallics* **2016**, *35*, 903.

(35) Francke, R.; Schille, B.; Roemelt, M. Homogeneously Catalyzed Electroreduction of Carbon Dioxide—Methods, Mechanisms, and Catalysts *Chem. Rev.* **2018**, *118*, 4631.

(36) (a) Buncel, E.; Menon, B. Carbanion mechanisms. 6. Metalation of arylmethanes by potassium hydride/18-crown-6 ether in tetrahydrofuran and the acidity of hydrogen *J. Am. Chem. Soc.* **1977**, *99*, 4457; (b) Morris, R. H. Brønsted–Lowry Acid Strength of Metal Hydride and Dihydrogen Complexes *Chem. Rev.* **2016**, *116*, 8588.

(37) The pK_a of H_2 in THF was first measured in ref 36a and a value of 35.5 was obtained. This was later refined to be ~ 49 (ref 36b). This gives a value of 66.8 +/- 1.4 kcal/mol for the free energy change associated with K_{H2-} which is used throughout this manuscript. A value of 68.7 kcal/mol was recently calculated and we report hydricities using the new value reported in the following reference in parentheses. Brereton, K; Jadrich, C.; Stratakes, B., Miller, A. J. M. *Organometallics*, **2019**, accepted.

(38) Tsay, C.; Livesay, B. N.; Ruelas, S.; Yang, J. Y. Solvation Effects on Transition Metal Hydricity *J. Am. Chem. Soc.* **2015**, *137*, 14114.

(39) Lilio, A. M.; Reineke, M. H.; Moore, C. E.; Rheingold, A. L.; Takase, M. K.; Kubiak, C. P. Incorporation of Pendant Bases into Rh(diphosphine)$_2$ Complexes: Synthesis, Thermodynamic Studies, And Catalytic CO_2 Hydrogenation Activity of $[Rh(P_2N_2)_2]^+$ Complexes *J. Am. Chem. Soc.* **2015**, *137*, 8251.

(40) Kütt, A.; Selberg, S.; Kaljurand, I.; Tshepelevitsh, S.; Heering, A.; Darnell, A.; Kaupmees, K.; Piirsalu, M.; Leito, I. pK_a values in organic chemistry – Making maximum use of the available data *Tetrahedron Lett.* **2018**, *59*, 3738.

(41) Kar, S.; Sen, R.; Goeppert, A.; Prakash, G. K. S. Integrative CO2 Capture and Hydrogenation to Methanol with Reusable

Catalyst and Amine: Toward a Carbon Neutral Methanol Economy *J. Am. Chem. Soc.* **2018**, *140*, 1580.

(42) Xie, Y.; Hu, P.; Ben-David, Y.; Milstein, D. A Reversible Liquid Organic Hydrogen Carrier System Based on Methanol-Ethylenediamine and Ethylene Urea *Angew. Chem.* **2019**, *131*, 5159.

(43) (a) Kortunov, P. V.; Baugh, L. S.; Siskin, M.; Calabro, D. C. In Situ Nuclear Magnetic Resonance Mechanistic Studies of Carbon Dioxide Reactions with Liquid Amines in Mixed Base Systems: The Interplay of Lewis and Brønsted Basicities *Energy & Fuels* **2015**, *29*, 5967; (b) Kortunov, P. V.; Siskin, M.; Baugh, L. S.; Calabro, D. C. In Situ Nuclear Magnetic Resonance Mechanistic Studies of Carbon Dioxide Reactions with Liquid Amines in Non-aqueous Systems: Evidence for the Formation of Carbamic Acids and Zwitterionic Species *Energy & Fuels* **2015**, *29*, 5940.

(44) Pitman, C. L.; Brereton, K. R.; Miller, A. J. M. Aqueous Hydricity of Late Metal Catalysts as a Continuum Tuned by Ligands and the Medium *J. Am. Chem. Soc.* **2016**, *138*, 2252.